SCIENCE CHINA Materials

ARTICLES

mater.scichina.com link.springer.com

Published online 3 February 2016 | doi: 10.1007/s40843-016-0120-3
Sci China Mater 2016, 59(2): 95–103

Hollow spherical $LiNi_{0.5}Mn_{1.5}O_4$ built from polyhedra with high-rate performance via carbon nanotube modification

Luoluo Wang, Zhengyao Hu, Kangning Zhao, Yanzhu Luo, Qiulong Wei, Chunjuan Tang, Ping Hu, Wenhao Ren and Liqiang Mai*

ABSTACT Lithium nickel manganese oxide spinel ($LiNi_{0.5}Mn_{1.5}O_4$, LNMO) has attracted much attention as the cathode material for rechargeable lithium-ion batteries due to its high energy density and low cost. However, the short cycle life and poor high-rate capability hinder its commercialization. In this study, we synthesized hollow spherical LNMO built from polyhedral particles. The LNMO hollow structure guarantees sufficient contact with electrolyte and rapid diffusion of lithium ions. To enhance the conductivity, we use carbon nanotubes (CNTs) to modify the surface of the cathode. After CNT modification, the LNMO hollow structure manifests outstanding cycling stability and high-rate capability. It delivers a discharge capacity of 127 mA h g^{-1} at 5 C, maintaining 104 mA h g^{-1} after 500 cycles. Even at a high rate of 20 C, a capacity of 121 mA h g^{-1} can be obtained. The excellent electrochemical performance is ascribed to the unique structure and the enhanced conductivity through CNT modification. It is demonstrated that the CNT-modified hollow spherical LNMO is a promising cathode for lithium ion batteries.

Keywords: lithium nickel manganese oxide spinel, hollow sphere, carbon nanotube modification, high-rate performance, lithium-ion batteries

INTRODUCTION

Lithium-ion batteries (LIBs) have been rapidly developed for the application in hybrid electric vehicles (HEVs) and electric vehicles (EVs) due to their high energy density and durable cyclability. The current commercialized olivine $LiFePO_4$ and layered $LiCoO_2$ are limited by their low energy density. One of the available strategies to increase the energy density is pursuing the high-voltage cathode. The high-voltage spinel $LiNi_{0.5}Mn_{1.5}O_4$ (LNMO) has been extensively investigated because of its high energy density [1]. The high working plateau (4.75 V *vs.* Li^+/Li) is the most distinct advantage of LNMO [2]. Combining with the theoretical specific capacity (147 mA h g^{-1}), the LNMO cathode can afford a high energy density of 658 W h kg^{-1}, which is higher than the traditional $LiCoO_2$ (620 W h kg^{-1}) and $LiFePO_4$ (591 W h kg^{-1}) cathode materials [3]. However, some drawbacks such as the fast capacity fading at high voltage [4] and the appearance of rock-salt phase at high temperature [5] limit the commercialization of LNMO.

It has been widely acknowledged that the electrochemical property of electrode materials is strongly related to the particle size, crystallinity and morphology [6]. To improve the performance, a wide variety of nanostructured electrodes, such as nanorods [7], porous structures [8], hollow microcubes and microspheres [9], and core-shell microspheres [10], have been designed and utilized in LIBs. Among these nanostructures, the porous and hollow structures can increase the contact area between the electrode and electrolyte, which is beneficial to reduce the transport path of lithium ions. Zhu *et al.* [11] reported the synthesis of LNMO microspheres with larger pores, which exhibited excellent performance. Luo *et al.* [12] synthesized LNMO hollow microspheres with excellent cycling stability and rate capability, which was attributed to the short electronic/ionic diffusion distance and accommodated volume change derived from the hollow structure. Li *et al.* [13] designed uniform $LiNi_{1/3}Mn_{1/3}Co_{1/3}O_2$ hollow microspheres with improved performance by using porous $Mn_{1.5}Co_{1.5}O_4$ microspheres as the template. All these literatures demonstrate that the rational structural design can significantly improve the electrochemical performance.

The cycling performance and high-rate capability are highly dependent on the conductivity of electrode materials [14]. Surface modification has been proved to be an efficient strategy to enhance electronic conductivity [15]. Among all modifying materials, carbon nanotube (CNT) is an ideal high electronic conducting material. It can efficiently improve the sluggish electron transportation and

State Key Laboratory of Advanced Technology for Materials Synthesis and Processing, Wuhan University of Technology, Wuhan 430070, China
* Corresponding author (email: mlq518@whut.edu.cn)

thus reduce the polarization of the electrodes. Ban *et al.* [16] synthesized 5 wt.% CNT-modified $LiNi_{0.4}Mn_{0.4}Co_{0.2}O_2$, which demonstrated excellent high-rate capability due to the fast diffusion of ions and electrons during cycling. Wu *et al.* [17] developed a fully active and depolarized composite cathode material based on $LiNi_{0.5}Mn_{0.3}Co_{0.2}O_2$ particles embedded in interwoven three-dimensional (3D) CNT network, which served as the superhighway for the electron and Li ion migration. Thang *et al.* [18] successfully functionalized CNTs by a mixture of H_2SO_4/HNO_3, and the CNTs were used as conducting addition to prepare $LiMn_2O_4$/CNT and LNMO/CNT. The nanocomposites cathodes displayed good capability when the content of CNT was 10%. Herein, CNTs are chosen as the surface modifying material to improve the performance of the as-prepared LNMO.

In this study, we synthesized pristine LNMO by a facile hydrothermal method followed by high temperature calcination. The hollow spherical structure can be obtained via controlling the calcination temperature. After CNT modification, the LNMO is surrounded by 3D continuous CNT network (denoted as LNMO-850/CNT). Structural characterization and electrochemical performance measurements were carried out to investigate the influence of CNT modification on the structure and properties of LNMO. The results illustrate that LNMO-850/CNT manifests high cycling stability (capacity retention of 82% after 500 cycles at 5 C) and excellent high-rate capability (121 mA h g^{-1} at 20 C).

EXPERIMENTAL

Synthesis

The pristine LNMO material was synthesized via a simple hydrothermal method followed by annealing. The stoichiometric amount of $MnSO_4{\cdot}H_2O$ (4.5 mmol) and $NiSO_4{\cdot}6H_2O$ (1.5 mmol) were dissolved 20 mL distilled water and 10 mL ethanol to form solution A. 30 mmol NH_4HCO_3 was dissolved in 20 mL distilled water to form solution B. Then, solution A and solution B was added simultaneously into 10 mL distilled water. After stirring at room temperature for 1 h, the mixture was transferred into a 100 mL Teflon-lined autoclave (200°C for 32 h). The precipitates were washed six times with deionized water and dried in a vacuum oven at 80°C for 12 h to get the laurel-green powder (carbonate precursor).

Afterwards, the carbonate precursor was presintered at 500°C for 5 h to obtain the corresponding oxides. $LiOH{\cdot}H_2O$ (with 5% Li excess) and oxides were dispersed in 30 mL ethanol. After stirring for 5 h, the mixture was dried at 85°C. The obtained powders were sintered at 800, 850, and 900°C for 16 h in air to obtain the LNMO samples, which were labeled as LNMO-800, LNMO-850, and LNMO-900, respectively. For the preparation of CNT modified sample, LNMO-850 was mixed with 5 wt.% of CNT in ethanol. After an ultrasonic treatment for 2 h, the mixture was dried at 85°C under continuous stirring to get the final product (designated as LNMO-850/CNT).

Characterizations

The thermogravimetric (TG) analysis and differential scanning calorimetry (DSC) measurements were carried out on a simultaneous thermal analyzer (STA 449 F3, NETZSCH) in air between 25 and 800°C at the heating rate of 10°C min^{-1}. The crystal structures of the samples were studied by X-ray powder diffraction (XRD, Bruker D8 Advance) with non-monochromated Cu Kα X-ray source. Fourier transform infrared spectroscopy (FT-IR) measurements were performed on a Nicolet 6700 spectrometer in transmission mode with a spectral resolution of 4 cm^{-1}. The morphologies and element mappings of the samples were characterized by field emission scanning electron microscopy (FESEM, JEOL JSM-7100F, 10kV) and high-resolution transmission electron microscopy (HRTEM, JEOL JEM-2100F, 200kV).

Electrochemical measurements

Electrochemical charge/discharge tests were performed by using CR2025-type coin cells with lithium metal as the anode. To prepare the working electrodes, active materials (70 wt.%) were mixed with Super P (20 wt.%), and polyvinylidene fluoride (PVDF, 10 wt.%) in *N*-methyl pyrrolidone (NMP) to obtain the slurry. After coating the slurry onto aluminum foil, the cathode was dried at 80°C overnight. The mass of each electrode is calculated within the range of 1.9–2.6 mg cm^{-2}, eliminating the mass loading of aluminum foil. With 1 mol L^{-1} $LiPF_6$ dissolved in ethylene carbonate (EC) and dimethyl carbonate (DMC) (1:1 by volume) as the electrolyte and Celgard 2400 membrane as the separator, the coin cell was assembled in an argon-filled glove box, in which O_2 and H_2O content were below 0.1 ppm. The capacity is calculated based on the total mass of the sample/composite.

The galvanostatic charge/discharge tests were performed between 3.0 and 4.9 V (*vs.* Li/Li^+) at different current densities on a LAND CT2001A battery testing system. Cyclic voltammetry (CV) curves were measured in the voltage range from 3.5 to 4.9 V on an electrochemical workstation (CHI 760D) at the scan rate of 0.1 mV s^{-1}. Electrochemical impedance spectroscopy (EIS) was carried out in a fre-

quency range from 100 kHz to 0.01 Hz at 10 mV on an electrochemical workstation (Auto lab).

RESULTS AND DISCUSSION

TG-DSC was employed to investigate the effects of calcination temperature on the precursor obtained through hydrothermal method. Fig. S1 shows the TG-DSC curves heating from 25 to 800°C in air. The TG curve indicates that there is an evident weight loss (19.3 wt.%) between 151 and 253°C due to the evaporation of surface-absorbed water. Another obvious weight loss (34.71 wt.%) observed from 253 to 332°C can be attributed to the decomposition of the carbonate, which is supported by exothermic peak around 305°C from DSC curve [19,20]. The weight lose above 350°C is negligible, indicating that the oxides have been obtained. Via the analysis of the TG-DSC results, the presintering temperature is chosen at 500°C, which not only assures the complete decomposition of the precursor, but also affords the excellent crystallinity of the oxides.

Fig. 1a displays the XRD patterns of the pristine LNMO-850 and LNMO-850/CNT, while the XRD patterns of LNMO-800 and LNMO-900 are shown in Fig. S2. It can be seen that all diffraction peaks are well in agreement with spinel LNMO (JCPDS No.80-2162) with $Fd\bar{3}m$ space group, in which the transition metal ions disorderly distribute at octahedral (16d) sites [21]. No impurities can be found in the patterns, suggesting the high purity of the samples.

FT-IR has been demonstrated to be an effective method to survey the degree of Mn and Ni cations disordering in LNMO [22,23]. The spectrum of the disordered phase ($Fd\bar{3}m$) is composed of several broad and undiscernable bands at 428, 465, 555 cm^{-1} [24], while the ordered phase ($P4_332$) has eight obvious bands because of the decreased space symmetry. In the ordered phase, the intensity of peaks at 428, 465, 555 cm^{-1} would increase distinctly [25]. The FT-IR spectra of LNMO sintered at different temperatures are shown in Fig. 1b. There are obvious peaks at 621 and 582 cm^{-1}, which are attributed to the vibrations of the Mn–O and Ni–O bands, respectively. The unconspicuous peaks at 428, 465, 555 cm^{-1} indicate that the disordered $Fd\bar{3}m$ structure is dominated in the lattice. Previous reports [26,27] indicated that the increase of Mn–O peak (621 cm^{-1}) and the decrease of Ni–O peak (582 cm^{-1}) can be attributed to the increasing degree of lattice disordering. The LNMO-900 displays a higher I_{621}/I_{582} ratio than the other samples, which indicates a slightly higher disordering degree in LNMO-900 with more Mn^{3+}.

The morphologies of LNMO samples were examined by FESEM. It can be observed from Fig. S3a that ideal spherical precursors are obtained after hydrothermal treatment. The spherical precursors are solid with sizes of 1 to 3 μm and they are composed of numerous nanoparticles. After presintering at 500°C, the oxides well maintain the solid spherical morphology (Fig. S3b). The elemental mappings in Fig. S3c indicate the homogeneous distribution of Ni, Mn, and O in the oxides. Starting from the same oxide precursor, the morphology of LNMO can be adjusted by tuning the sintering temperature. The spherical LNMO-800 is composed of a compact shell and a loosely stacked by nanoparticulate core in the center (Fig. 2a). After increasing the annealing temperature, the LNMO-850 (Fig. 2b) shows a hollow spherical structure (3–5 μm) built from numerous polyhedral particles with the sizes of 200–300 nm. The structure of polyhedral nanoparticles on the surface of LNMO-850 can be seen clearly on Fig. S3d. Element mapping results (Fig. S3e) indicate that the Ni, Mn, and O elements distribute homogeneously in the LNMO sample. The

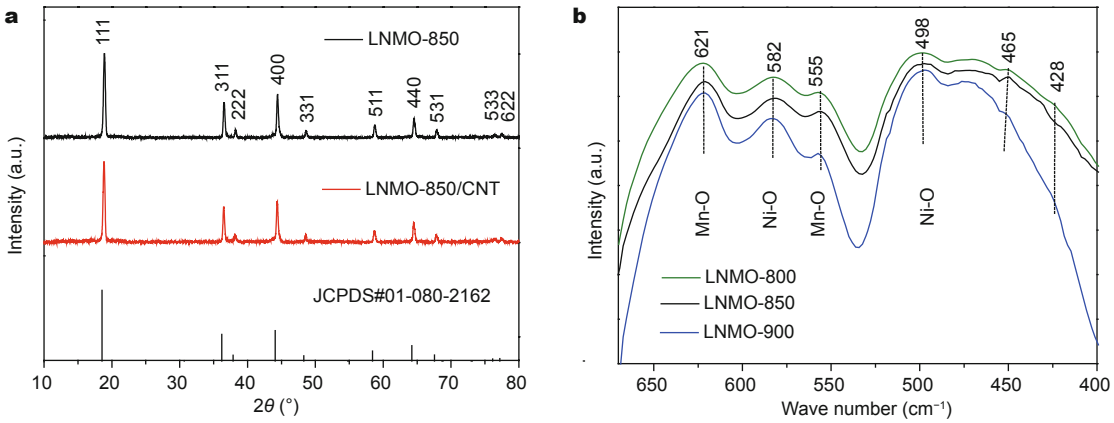

Figure 1 (a) XRD patterns of LNMO-850 and LNMO-850/CNT; (b) FT-IR spectra of LNMO synthesized at different temperatures.

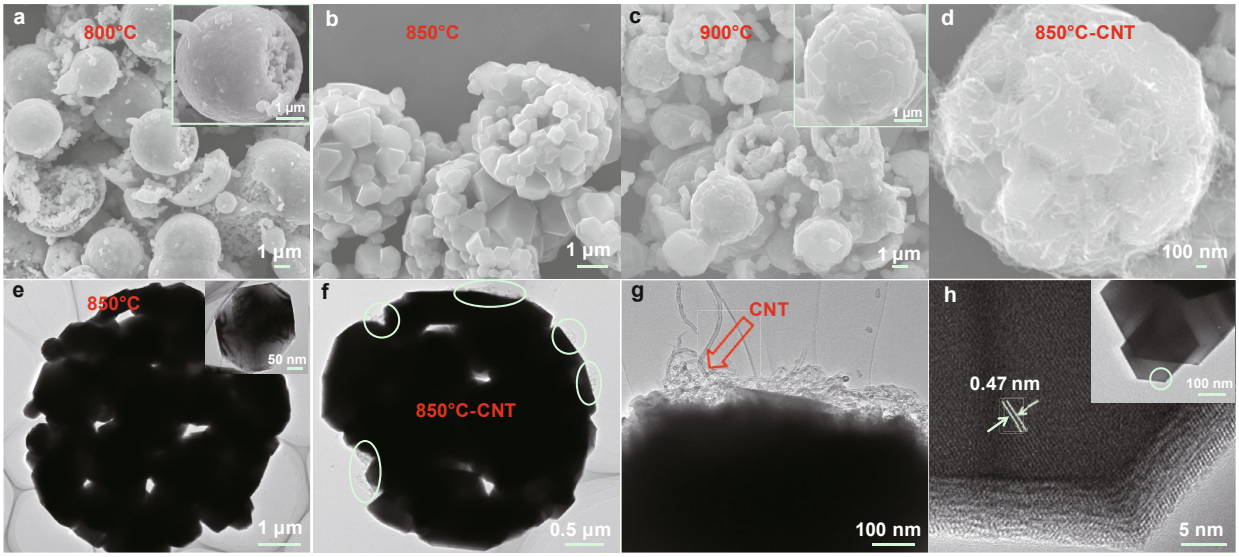

Figure 2 SEM images of (a) LNMO-800, (b) LNMO-850, (c) LNMO-900, and (d) LNMO-850/CNT, TEM images of (e) LNMO-850, (f, g) LNMO-850/CNT, and (h) HRTEM images of LNMO-850.

hollow spherical structure can be maintained at even higher temperature (900°C). However, the LNMO-900 shows a thick and compact shell due to the growth of polyhedral particles at high temperature (Fig. 2c). CNTs are used to modify the LNMO-850. The surface of LNMO-850/CNT becomes rough after the CNT modification (Fig. 2d). The low magnification SEM image and the corresponding elemental mappings are shown in Fig. S3f, which unambiguously demonstrates the homogeneous distribution of CNTs on the LNMO surface. The content of CNT in LNMO-850/CNT is determined to be 4.96 wt.%, which is in highly consistent with the theoretical value of 5.0 wt.%.

Fig. S3g shows the spherical morphology of LNMO-850, and the TEM image in Fig. 2e is used to further confirm the hollow spherical structure of LNMO-850. The uniform distributions of holes on the image prove the hollow structure combined with SEM images. The inset of Fig. 2e shows that the primary particle has a polyhedral shape with the size ranges of 200–300 nm, which is consistent with the SEM image. The polyhedral particle owns fourteen exposed planes. The CNTs can be clearly observed on the surface of LNMO-850/CNT (Figs 2f and g). The high resolution TEM (HETEM) image of LNMO-850 is shown in Fig. 2h, from which the (111) lattice fringes with interplanar spacings of 0.47 nm can be clearly observed.

As shown in the SEM and TEM images, the morphology of LNMO is highly dependent on the sintering temperature. The schematic illustrations are displayed in Fig. 3a. The precursors are solid spheres built from nanoscale particles. The spaces between nanoparticles in the oxides are enlarged due to the release of carbon dioxide, providing an appropriate space accommodation of LiOH. The homogeneous distribution of LiOH in the oxides facilitates the subsequent solid state reaction and LNMO formation. When sintered at 800°C, the gradually growing nanoparticles are enveloped by relatively compact shell. The interparticle spaces are further enlarged, which is attributed to the opposite diffusion of O atom and transition metal atoms [28,29]. This LNMO sphere with porous core and compact shell is gradually transformed into hollow spherical structure with the increasing of temperature. When sintered at 850°C, hollow spherical structure built from polyhedral particles is obtained. The fast outward diffusion of Mn and Ni atoms and the slow inward diffusion of O atom are responsible for the formation of the hollow cavity in LNMO-850 [28,29]. At 900°C, the growth of polyhedral particles leads to the formation of hollow spherical structure with thick and compact wall (Fig. 2c).

Although all samples inherit the spherical morphology from the carbonate precursor, only LNMO-850 shows a hollow spherical structure with porous shell. It is expected that this structure can guarantee sufficient contact between the electrode material and electrolyte, which effectively shortens the diffusion path of lithium ions [11]. Moreover, the hollow spherical structure can accommodate the volume change during repeated Li^+ insertion/extraction processes, resulting in a considerable improvement in the cycling stability [9,30,31]. The schematic illustration of a single polyhedral particle is also shown in Fig. 3a. The polyhedral particle has fourteen exposed planes (six quad-

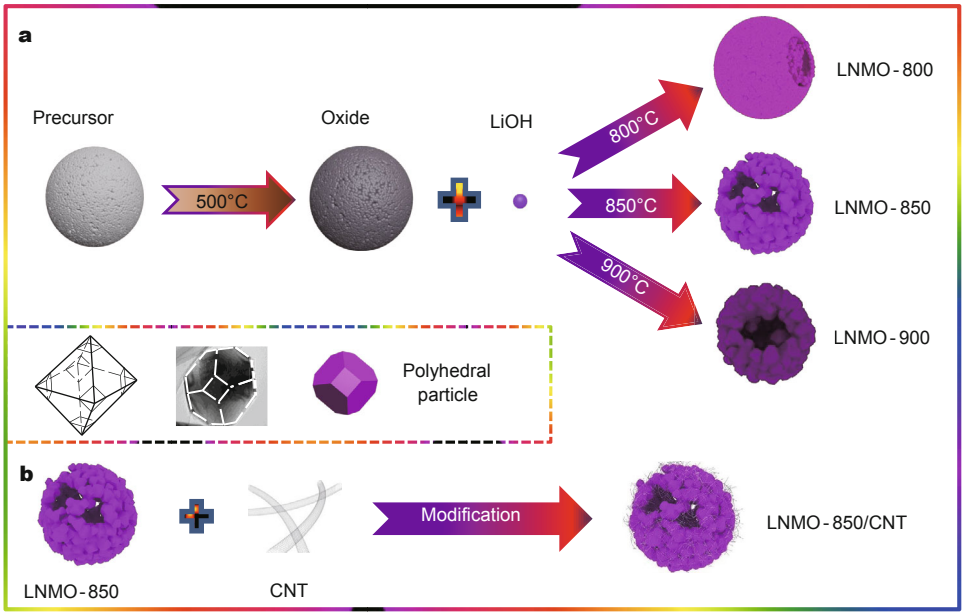

Figure 3 Schematic illustration of (a) hollow spherical LNMO built from polyhedral particles under different temperatures, (b) CNT modification process.

rangles and eight hexagons), which can be described via cutting the six vertices of an octahedron. The migrating route of lithium ions can be shortened by this nanoscale polyhedral structure. Fig. 3b illustrates the process for CNT modification of LNMO-850. The CNT modification on the surface of LNMO-850 forms a continuous 3D conducting network, which significantly enhances the conductivity of the LNMO [32].

Cyclic voltammetry (CV) was employed to understand the electrochemical reaction processes. Fig. 4a manifests the CV curves of all samples at the scan rate of 0.1 mV s^{-1} between 3.5–4.9 V. All samples exhibit two pairs of peaks at around 4.7 V, which can be attributed to the Ni^{2+}/Ni^{3+} and Ni^{3+}/Ni^{4+} redox pairs [33,34]. Minor redox peaks (inset of Fig. 4a) can also be observed at around 4.0 V in all samples, which are ascribed to the redox couple of Mn^{3+}/Mn^{4+} [35]. Among the three samples prepared at different temperatures, LNMO-900 has the most obvious redox peaks at around 4.0 V. This phenomenon is possibly related to the increased quantity of Mn^{3+} ions during high temperature calcination. According to previous literatures, the existence of Mn^{3+} is beneficial to the conductivity of LNMO [36]. Table S1 summarizes the voltage differences between the redox peaks. The minimum voltage difference is achieved for LNMO-900, indicating the minimized polarization among the three samples. However, the peak area of LNMO-900 is smaller than that of LNMO-850, suggesting the lower capacity of LNMO. Hence, the LNMO-850 is chosen as the standard sample to be modified with CNTs. After CNT modification, LNMO-850/CNT has better resolved redox peaks and minor voltage difference than LNMO-850, indicating the smaller polarization.

The rate performances at 0.5–20 C are displayed in Fig. 4b. The samples are cycled for 10 cycles at each rate. In general, the LNMO-850/CNT shows the best rate performance among all samples. The LNMO-850/CNT delivers a capacity of 138 mA h g^{-1} at 0.5 C, and there is almost no capacity decay with the increase of charge/discharge current to 1 and 2 C, suggesting the excellent rate capability. At 20 C, the discharge capacity of LNMO-850/CNT still remains at 121 mA h g^{-1}, while the capacities of LNMO-800, LNMO-850, LNMO-900 decrease to 78, 105, 99 mA h g^{-1}, respectively. When the rate is reduced to 0.5 C after the high rate testing, a capacity of 136 mA h g^{-1} (99% of capacity at initial 0.5 C) can be recovered for LNMO-850/CNT, which is the best among all samples. The discharge curves of LNMO-850/CNT at different rates are shown in Fig. S4a. Below 5 C, well defined discharge plateaus can be observed at about both 4.7 V and 4.0 V. At higher rates, the high discharge plateau associated with the Ni^{2+}/Ni^{4+} redox couple can still be seen distinctly at about 4.5 V. The excellent rate capability of LNMO-850/CNT can be ascribed to the synergistic effect of hollow-spherical structure and the CNT modification on the surface.

The charge/discharge profiles at 5 C for all samples are shown in Fig. 4c. All samples exhibit quite similar charge/

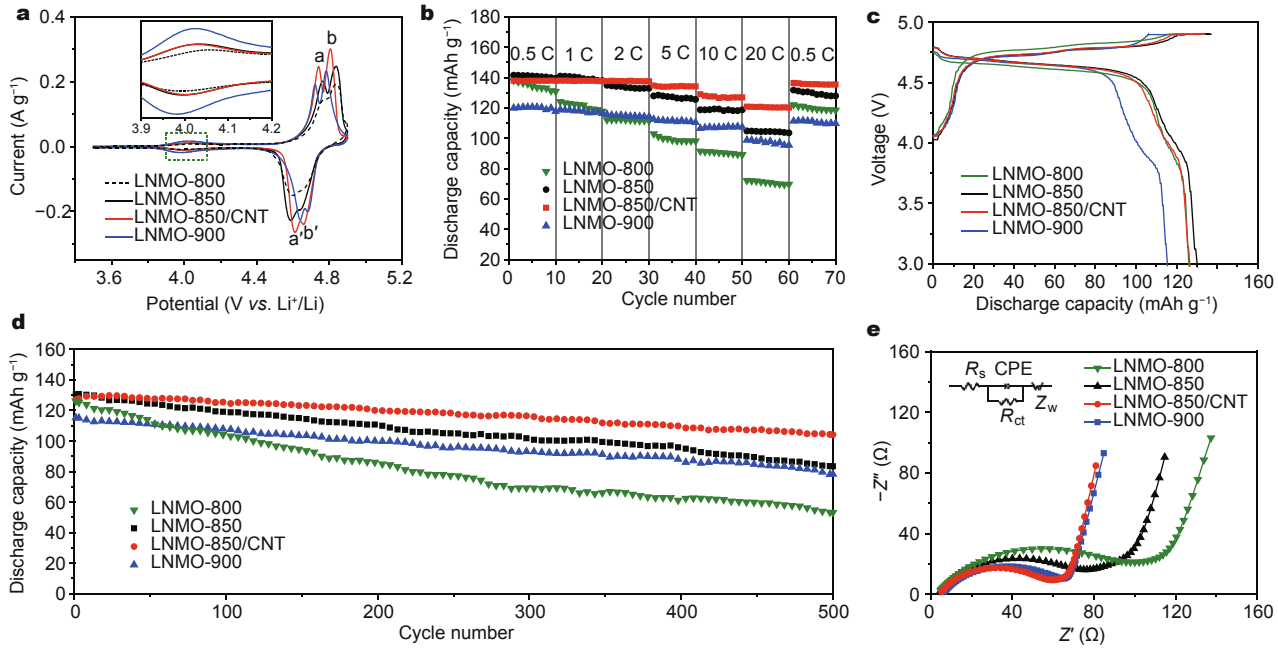

Figure 4 Electrochemical performances of LNMO synthesized at different temperatures: (a) CV curves, (b) rate capability, (c) charge/discharge curves at 5 C; (d) cycling performances at 5 C in the voltage range of 3.0–4.9 V; (e) EIS of LNMO-800, LNMO-850, LNMO-850/CNT and LNMO-900.

discharge profiles with two plateaus. The primary plateau at about 4.7 V is associated with the Ni^{2+}/Ni^{4+} redox couple, while the minor plateau at around 4.0 V is associated with the Mn^{3+}/Mn^{4+} redox couple [35]. Among all samples, LNMO-850/CNT has the smallest potential difference between the charge/discharge plateaus. This indicates the minimized polarization during the electrochemical reaction. The LNMO-850/CNT delivers an initial capacity of 127 mA h g^{-1}, which is a little bit lower than that of LNMO-850 (131 mA h g^{-1}). The slightly lower initial capacity of LNMO-850/CNT is due to the addition of CNTs, which contributes no capacity. The charge/discharge profiles of LNMO-850 and LNMO-850/CNT at other C rates are shown in Figs S4b–d, which also demonstrate the enhanced conductivity by CNT modification. The power density and energy density of LNMO-850 and LNMO-850/CNT are shown in Fig. S5. The samples both exhibit high energy and power density, among which the LNMO-850/CNT owns the energy density of 619 W h kg^{-1} and the power density of 0.4 kW kg^{-1} when discharging at 0.5 C.

Fig. 4d shows the cycling performances at 5 C. Among the three samples obtained at different temperatures, LNMO-850 delivers the highest initial capacity (131 mA h g^{-1}). The discharge capacities of LNMO-800 and LNMO-900 are 126, 115 mA h g^{-1} respectively. After 500 cycles, the capacities decrease to 83, 53, 79 mA h g^{-1} for LNMO-850, LNMO-800, LNMO-900, respectively. The capacity fading of LNMO-800 (57.9%) is more serious than that of LNMO-850 (35.9%) and LNMO-900 (31.3%), which is due to the unsatisfactory crystallinity of LNMO-800. Due to the highest crystallinity and Mn^{3+} concentration, LNMO-900 displays the best capacity retention [36]. However, the discharge capacity of LNMO-900 is considerably lower than the other two samples. This might be attributed to the formation of inactive rock-salt phases during the calcination at high temperature [37]. That is to say, the reduction of Mn^{4+} to Mn^{3+} is accompanied by the formation of rock-salt impurities; the formation of Mn^{3+} enhances the conductivity, while the formation of rock-salt impurities sacrifices the capacity. Overall, the LNMO-850 shows the best tradeoff between capacity and capacity retention. After CNT modification, the LNMO-850/CNT manifests a cycling performance superior to LNMO-850. An initial capacity of 127 mA h g^{-1} is obtained, maintaining 104 mA h g^{-1} after 500 cycles. The capacity fading is as low as 0.036% per cycle. Compared with the previous reports, the LNMO-850/CNT shows better electrochemical performance, especially excellent cycling performance and high-rate capability [18,38]. The outstanding cycling stability of LNMO-850/CNT is attributed to (1) the hollow and porous

structure for volume variation accommodation, (2) small size of polyhedral particles for solid state Li^+ diffusion, and (3) the improved conductivity via CNT modification.

To better understand the substantial difference between the samples, EIS was adopted. Fig. 4e shows the impedance spectra of all samples before cycling. All samples possess a semicircle at high frequency region and an oblique line at low frequency region. The diameter of the semicircle represents the charge transfer resistance (R_{ct}) and the slope of the line indicates the solid-state diffusion of Li^+ ions in the electrode [39,40]. The LNMO-850/CNT displays the lowest charge transfer resistance with the fitting value of 50.5 Ω, while the LNMO-800, LNMO-850, LNMO-900 have R_{ct} values of 85.5, 65.1, 58.1 Ω, respectively. The low charge transfer resistance of LNMO-850/CNT can be attributed to the high conductivity of CNTs, which serve as the highway for electron transfer.

Our results show that the LNMO-850/CNT possesses outstanding cycling stability and rate performance. The excellent electrochemical performance can be attributed to three factors: (1) the pores among the loosely stacked polyhedral particles provide sufficient contact between the electrode and electrolyte, which efficiently shortens the diffusion path of lithium ions. (2) The hollow and porous structure can effectively accommodate the volume change during repeated Li^+ insertion/extraction processes, which leads to considerable improvement in cycling performance. (3) The CNT modification on the surface can form a 3D continuous network for electron transfer, which significantly enhances the rate capability.

CONCLUSIONS

Hollow spherical LNMO was successfully synthesized via a facile hydrothermal method followed by sintering. The annealing temperature significantly affects the morphology and electrochemical performances of LNMO. The hollow spherical structure built from polyhedral nanoparticles can be obtained at a calcination temperature of 850°C. After CNT modification, the LNMO-850/CNT manifests outstanding cycling stability and rate capability. It delivers an initial discharge capacity of 127 mA h g^{-1} at 5C, maintaining 104 mA h g^{-1} after 500 cycles. The capacity fading is as low as 0.036% per cycle. At an even higher rate of 20 C, a discharge capacity of 121 mA h g^{-1} can be maintained. The excellent electrochemical performance can be attributed to the reduced diffusion path for lithium ions originated from the porous hollow spherical structure, the well-accommodated volume variation during repeated lithium insertion/extraction, and the enhanced electronic conductivity resulting from the introduction of 3D CNT network on the surface. The outstanding electrochemical performance makes the CNT modified LNMO a promising cathode for high-energy lithium-ion batteries.

Received 8 January 2016; accepted 2 February 2016; published online 3 February 2016

1 Yang L, Ravdal B, Lucht BL. Electrolyte reactions with the surface of high voltage $LiNi_{0.5}Mn_{1.5}O_4$ cathodes for lithium-ion batteries. Electrochem Solid State Lett, 2010, 13: A95–A97
2 Santhanam R, Rambabu B. Research progress in high voltage spinel $LiNi_{0.5}Mn_{1.5}O_4$ material. J Power Sources, 2010, 195: 5442–5451
3 Ma X, Kang B, Ceder G. High rate micron-sized ordered $LiNi_{0.5}Mn_{1.5}O_4$. J Electrochem Soc, 2010, 157: A925–A931
4 Wang Y, Yang G, Yang Z, *et al*. High power and capacity of $LiNi_{0.5}Mn_{1.5}O_4$ thin films cathodes prepared by pulsed laser deposition. Electrochim Acta, 2013, 102: 416–422
5 Xiao J, Chen X, Sushko PV, *et al*. High-performance $LiNi_{0.5}Mn_{1.5}O_4$ spinel controlled by Mn^{3+} concentration and site disorder. Adv Mater, 2012, 24: 2109–2116
6 Lou XW, Archer LA, Yang Z. Hollow micro/nanostructures: synthesis and applications. Adv Mater, 2008, 20: 3987–4019
7 Yang J, Zhang X, Zhu Z, Cheng F, Chen J. Ordered spinel $LiNi_{0.5}Mn_{1.5}O_4$ nanorods for high-rate lithium-ion batteries. J Electroanal Chem, 2013, 688: 113–117
8 Zhang X, Cheng F, Yang J, Chen J. $LiNi_{0.5}Mn_{1.5}O_4$ porous nanorods as high-rate and long-life cathodes for Li-ion batteries. Nano Lett, 2013, 13: 2822–2825
9 Zhou L, Zhao D, Lou XD. $LiNi_{0.5}Mn_{1.5}O_4$ hollow structures as high-performance cathodes for lithium-ion batteries. Angew Chem Int Ed, 2012, 51: 239–241
10 Jo M, Lee YK, Kim KM, Cho J. Nanoparticle-nanorod core-shell $LiNi_{0.5}Mn_{1.5}O_4$ spinel cathodes with high energy density for Li-ion batteries. J Electrochem Soc, 2010, 157: A841–A845
11 Zhu X, Li X, Zhu Y, *et al*. Porous $LiNi_{0.5}Mn_{1.5}O_4$ microspheres with different pore conditions: preparation and application as cathode materials for lithium-ion batteries. J Power Sources, 2014, 261: 93–100
12 Luo H, Nie P, She L, *et al*. Synthesis of $LiNi_{0.5}Mn_{1.5}O_4$ hollow microspheres and their lithium-storage properties. ChemElectroChem, 2015, 2: 127–133
13 Li J, Xiong Y, Liu Y, Ju Z, Qian Y. Uniform $LiNi_{1/3}Co_{1/3}Mn_{1/3}O_2$ hollow microspheres: designed synthesis, topotactical structural transformation and their enhanced electrochemical performance. Nano Energy, 2013, 2: 1249–1260
14 Feng XY, Shen C, Fang X, Chen CH. Synthesis of $LiNi_{0.5}Mn_{1.5}O_4$ by solid-state reaction with improved electrochemical performance. J Alloy Compd, 2011, 509: 3623–3626
15 Yang T, Zhang N, Lang Y, Sun K. Enhanced rate performance of carbon-coated $LiNi_{0.5}Mn_{1.5}O_4$ cathode material for lithium ion batteries. Electrochim Acta, 2011, 56: 4058–4064
16 Ban C, Li Z, Wu Z, *et al*. Extremely durable high-rate capability of a $LiNi_{0.4}Mn_{0.4}Co_{0.2}O_2$ cathode enabled with single-walled carbon nanotubes. Adv Energy Mater, 2011, 1: 58–62
17 Wu ZZ, Han XG, Zheng JX, *et al*. Depolarized and fully active cathode based on $Li(Ni_{0.5}Co_{0.2}Mn_{0.3})O_2$ embedded in carbon nanotube network for advanced batteries. Nano Lett, 2014, 14: 4700–4706
18 Thang VL, My LPL, Man VT, *et al*. Fabrication of cathode materials based on $LiMn_2O_4$/CNT and $LiNi_{0.5}Mn_{1.5}O_4$/CNT nanocomposites for lithium-ion batteries application. Mater Res, 2015, 18: 1044–1052
19 Ohzuku T, Takeda S, Iwanaga M. Solid-state redox potentials

for $Li[Me_{1/2}Mn_{3/2}]O_4$ (Me: 3d-transition metal) having spinel-framework structures: a series of 5 volt materials for advanced lithium-ion batteries. J Power Sources, 1999, 81–82: 90–94
20 Xu HY, Xie S, Ding N, *et al*. Improvement of electrochemical properties of $LiNi_{0.5}Mn_{1.5}O_4$ spinel prepared by radiated polymer gel method. Electrochim Acta, 2006, 51: 4352–4357
21 Kim JH, Myung ST, Yoon CS, Kang SG, Sun YK. Comparative study of $LiNi_{0.5}Mn_{1.5}O_{4-\delta}$ and $LiNi_{0.5}Mn_{1.5}O_4$ cathodes having two crystallographic structures: $Fd\bar{3}m$ and $P4_332$. Chem Mater, 2004, 16: 906–914
22 Amdouni N, Zaghib K, Gendron F, Mauger A, Julien CM. Structure and insertion properties of disordered and ordered $LiNi_{0.5}Mn_{1.5}O_4$ spinels prepared by wet chemistry. Ionics, 2006, 12: 117–126
23 Ivanova S, Zhecheva E, Stoyanova R, *et al*. High-voltage $LiNi_{0.5}Mn_{1.5}O_4$ spinel: cationic order and particle size distribution. J Phys Chem C, 2011, 11: 25170–25182
24 Kunduraci M, Amatucci GG. Synthesis and characterization of nanostructured 4.7 V Li_x $Ni_{0.5}Mn_{1.5}O_4$ spinels for high-power lithium-ion batteries. J Electrochem Soc, 2006, 153: A1345–A1352
25 Ariyoshi K, Iwakoshi Y, Nakayama N, Ohzuku T. Topotactic two-phase reactions of $Li[Ni_{1/2}Mn_{3/2}]O_4$ ($P4_332$) in nonaqueous lithium cells. J Electrochem Soc, 2004, 151: A296–A303
26 Kunduraci M, Al-Sharab JF, Amatucci GG. High-power nanostructured $LiMn_{2-x}Ni_xO_4$ high-voltage lithium-ion battery electrode materials: electrochemical impact of electronic conductivity and morphology. Chem Mater, 2006, 18: 3585–3592
27 Zhu Z, Yan H, Zhang D, Li W, Lu Q. Preparation of 4.7 V cathode material $LiNi_{0.5}Mn_{1.5}O_4$ by an oxalic acid-pretreated solid-state method for lithium-ion secondary battery. J Power Sources, 2013, 224: 13–19
28 Lou XW, Lynden AA, Yang ZC. Hollow micro/nanostructures: synthesis and applications. Adv Mater, 2008, 20: 3987–4019
29 Jung SC, Young JH, Yun CK. Design and synthesis of bubble-nanorod-structured Fe_2O_3-carbon nanofibers as advanced anode material for Li-ion batteries. ACS Nano, 2015, 9: 4026–4035
30 Deng Y, Zhou Y, Shi Z, Zhou X, Quan X. Porous $LiMn_2O_4$ microspheres as durable high power cathode materials for lithium ion batteries. J Mater Chem A, 2013, A1: 8170–8177
31 Liu J, Hou M, Yi J, *et al*. Improving the electrochemical performance of layered lithium-rich transition-metal oxides by controlling the structural defects. Energy Environ Sci, 2014, 7: 705–714
32 Fang X, Ge MY, Rong JP, Zhou CW. Free-standing $LiNi_{0.5}Mn_{1.5}O_4$/carbon nanofiber network film as lightweight and high-power cathode for lithium ion batteries. ACS Nano, 2014, 8: 4876–4882
33 Yoon T, Park S, Mun J, *et al*. Failure mechanisms of $LiNi_{0.5}Mn_{1.5}O_4$ electrode at elevated temperature. J Power Sources, 2012, 215: 312–316
34 Sun Y, Yang Y, Zhan H, Shao H, Zhou Y. Synthesis of high power type $LiNi_{0.5}Mn_{1.5}O_4$ by optimizing its preparation conditions. J Power Sources, 2010, 195: 4322–4326
35 Lee ES, Nam KW, Hu E, Manthiram A. Influence of cation ordering and lattice distortion on the charge-discharge behavior of $LiNi_{0.5}Mn_{1.5}O_4$ spinel between 5.0 and 2.0 V. Chem Mater, 2012, 24: 3610–3620
36 Cabana J, Casas-Cabanas M, Omenya FO, *et al*. Composition-structure relationships in the Li-ion battery electrode material $LiNi_{0.5}Mn_{1.5}O_4$. Chem Mater, 2012, 24: 2952–2964
37 Lv YZ, Jin YZ, Xue Y, *et al*. Electrochemical properties of high-voltage $LiNi_{0.5}Mn_{1.5}O_4$ synthesized by a solid-state method. RSC Adv, 2014, 4: 26022
38 Cheng JL, Li XH, Wang ZX, *et al*. Hydrothermal synthesis of $LiNi_{0.5}Mn_{1.5}O_4$ sphere and its performance as high-voltage cathode material for lithium ion batteries. Ceram Int, 2016, 42: 3715–3719
39 Kang HB, Myung ST, Amine K, Lee SM, Sun YK. Electrochemical properties of high-voltage $LiNi_{0.5}Mn_{1.5}O_4$ synthesized by a solid-state method. J Power Sources, 2010, 195: 2023–2028
40 Wu HM, Belharouak I, Abouimrane A, Sun YK, Amine K. Surface modification of $LiNi_{0.5}Mn_{1.5}O_4$ by ZrP_2O_7 and ZrO_2 for lithium-ion batteries. J Power Sources, 2010, 195: 2909–2913

Acknowledgements This work was supported by the National Basic Research Program of China (2013CB934103 and 2012CB933003), the International Science & Technology Cooperation Program of China (2013DFA50840), the National Natural Science Foundation of China (51521001 and 51272197), the National Natural Science Fund for Distinguished Young Scholars (51425204), Hubei Province Natural Science Fund for Distinguished Young Scholars (2014CFA035), and the Fundamental Research Funds for the Central Universities (WUT: 2015-III-032, 2015-III-021).

Author contributions Wang L, Hu Z and Mai L conceived the study. Wang L, Hu Z and Luo Y carried out the experiments. Wang L, Luo Y and Zhao K wrote the manuscript. Wei Q, Tang C, Hu P and Ren W modified the manuscript. All authors read and approved the final manuscript.

Conflict of interest The authors declare that they have no conflict of interest.

Supplementary information Supporting data are available in the online version of the paper.

Luoluo Wang received her bachelor degree from Southwest Jiaotong University in 2013. She is currently a graduate student at the State Key Laboratory of Advanced Technology for Materials Synthesis and Processing, Wuhan University of Technology. Her research interest focuses on nano energy cathode materials.

Liqiang Mai received his PhD degree from Wuhan University of Technology in 2004 and then worked as a postdoctoral researcher at Georgia Institute of Technology in the group of Prof. Zhonglin Wang from 2006 to 2007. He conducted nanowire based nanodevices and battery research as advanced research scholar in the group of Prof. Charles M Lieber at Harvard University from 2008 to 2011. He was the winner of the National Natural Sceince Fund for Distinguished Young Scholars in 2014. His current research field is nano energy materials and micro/nano devices. So far, he has published more than 130 papers tagged by SCI in leading journals.

碳纳米管改性的多面体颗粒自组装中空球状$LiNi_{0.5}Mn_{1.5}O_4$及其高倍率性能

王洛洛, 胡正耀, 赵康宁, 罗艳珠, 魏湫龙, 唐春娟, 胡平, 任文皓, 麦立强

摘要 本文通过调节烧结温度设计构筑了一种纳米多面体颗粒堆积的中空球状$LiNi_{0.5}Mn_{1.5}O_4$材料，并进一步通过碳纳米管(CNT)的改性来提高材料的循环性能和高倍率性能. 纳米中空结构不仅减少了锂离子的扩散路径，也保证了电解液和正极材料的充分接触，三维网状CNT的改性提高了材料的电子导电率，从而明显改善了材料的循环和高倍率性能. 最终得到的LNMO-850/CNT材料在5 C的电流密度下初始容量为127 mA h g^{-1}, 500次循环后容量保持在104 mA h g^{-1}. 而在20 C的高电流密度下容量仍达到121 mA h g^{-1}, 体现了材料优异的循环和高倍率性能.